Chemical Engineering Journal 160 (2010) 57–62

Contents lists available at ScienceDirect

Chemical Engineering Journal

journal homepage: www.elsevier.com/locate/cej

Arsenate removal from water using Fe_3O_4-loaded activated carbon prepared from waste biomass

Zhengang Liu[a,b], Fu-Shen Zhang[a,*], Ryo Sasai[b]

[a] Research Center for Eco-Environmental Sciences, Chinese Academy of Sciences, 18 Shuangqing Road, Beijing 100085, China
[b] EcoTopia Science Institute, Nagoya University, Furo-cho, Chikusa-ku, Nagoya 464-8603, Japan

ARTICLE INFO

Article history:
Received 12 October 2009
Received in revised form 27 February 2010
Accepted 1 March 2010

Keywords:
Waste biomass
Arsenic
Magnetization
Adsorption isotherm

ABSTRACT

A novel process for the preparation of Fe_3O_4-loaded activated carbon (MY) was developed using waste biomass. The key point of the synthetic strategy was that the carbonization, activation and Fe_3O_4 loading were accomplished simultaneously. The low-cost composite was characterized and used as an adsorbent for arsenate removal from water. The results showed that the Fe_3O_4 particles were uniformly deposited on the surface of the composite. The composite exhibited high surface area of 349 m^2/g, pore volume of 0.20 cm^3/g and iron of 39 wt.% for arsenate adsorption. As an adsorbent, higher temperature favored the adsorption capacity and the adsorption process was well fitted by pseudo-second-order model. The composite showed an excellent adsorption capability for arsenate with a maximum adsorption capacity of 204.2 mg/g at pH 8.0 and the adsorption process followed the Freundlich isotherm model well. In addition, the composite exhibited a saturation magnetization of 47.67 emu/g, which allowed it to be easily recovered by an external magnetic field after the adsorption process.

1. Introduction

Water pollution by arsenic has attracted increasing interest all over the world and due to its mobility and toxicity the arsenic pollution has been recorded by World Health Organization as a first priority issue. In the aquatic environments arsenic is primarily present in inorganic species (arsenate and arsenite) and arsenate (As(V)) is the predominant arsenic form in oxidizing conditions [1].

Thus far, several technologies including membrane filtration, coagulation and phytoremediation have been developed for arsenic removal from aqueous solutions, and adsorption is considered as an effective technology. Iron oxide has been proven to be an excellent adsorbent with high affinity toward inorganic arsenic species and selectivity in the adsorption process [2–4]. However, iron oxide is very bulky in nature, highly amorphous, and flocculant, which limits its widespread application for arsenic removal. To improve the adsorption efficiency, recent research has focused on creating media supporting iron oxide [5–7]. Among the tested supports, activated carbon was proven an ideal support because of its stable and variable pore property and promising results for As(V) removal were obtained using iron oxide-loaded activated carbons [8–11]. It was revealed that the effectiveness of the arsenic removal is closely related both to the amount of iron loaded and dispersion and surface accessibility of this iron within the activated carbon [12]. In particular, magnetic iron oxide-loaded activated carbon can also solve the notoriously difficult separation of activated carbon by using magnetic separation [13,14].

Unfortunately, to obtain these iron oxide-loaded activated carbon, the procedures are complicated and several single sequential steps, including parent material preparation, activated carbon oxidation and iron precursor impregnation, are needed [12]. In addition, the high cost of the activated carbon is another limiting factor for its widespread utilization. Under this situation, the process which enables preparation of iron-impregnated activated carbon through simple route and at low-cost is needed to be developed.

In the present study, we reported a novel and simple synthetic approach to produce Fe_3O_4-loaded activated carbon using the waste biomass. The produced composite was characterized and the adsorption capacity of As(V) was investigated to valuate its effectiveness for As(V)-contaminated wastewater treatment.

2. Experimental

2.1. Materials

Analytical grade sulfuric acid, nitric acid, sodium hydroxide and ferric chloride were purchased from Beijing Chemicals Company and $Na_2HAsO_4{\cdot}7H_2O$ was from Sigma–Aldrich. Waste biomass

* Corresponding author. Tel.: +86 10 62849515; fax: +86 10 62849515.
E-mail address: fszhang@rcees.ac.cn (F.-S. Zhang).

1385-8947/$ – see front matter © 2010 Elsevier B.V. All rights reserved.
doi:10.1016/j.cej.2010.03.003

Table 1
Chemical analysis of the pinewood sawdust used in the present study.

Elemental analysis (%)					Chemical composition (%)			Ash
C	H	O[a]	N	S	Cellulose	Hemicellulose	Lignin	
43.25	6.01	50.43	0.21	0.10	41	27	28	0.26

[a] By difference.

(pinewood sawdust) was obtained from a wood processing factory in Beijing suburb and the results of chemical analysis were shown in Table 1.

2.2. Preparation of the Fe_3O_4-loaded activated carbon composite

The sawdust was firstly dried at 378 K for 24 h in an oven, air cooled, and ground into dimensions ≤80 meshes. A proportion of 2 g of the sawdust sample and 20 ml 1.0 mol/L $FeCl_3$ solution were mixed followed by adding 10 ml 50% sulfuric acid. The resulting mixture was ultrasonicated for 2 h for thorough mixing and aged at 333 K for 12 h. Subsequently the slurry was subjected to centrifugal separation. The recovered residue was set on a quartz boat which was then inserted into a stainless tube and pyrolyzed in a horizontal pyrolysis reactor heated by electrical furnace. The sample was heated to 873 K within 115 min under 30 ml/min nitrogen gas and held at 873 K for 60 min. After cooling inside furnace under nitrogen atmosphere, the solid product was washed with de-ionized water until the filtrates were close to neutral. Subsequently the product was dried at 333 K for 24 h and then kept in a desiccator for use (designed as MY). Additionally, the product of the sawdust only impregnated with sulfuric acid was prepared under same procedure for comparison (designed as MN).

2.3. Characterization of the composite

The structure properties were determined by XRD (Shimadazu, Japan) using graphite monochromatic copper radiation over the 2θ range 10–80°. The BET surface areas were obtained from nitrogen adsorption isotherms at 77 K using an ASAP 2010 analyzer (Micromeritics, USA). The surface morphology was examined by scanning electron microscopy (S-3000, Japan) and X-ray mapping of Fe and O was performed using energy dispersive X-ray spectroscope (EDAX, USA) connected to the SEM. The MY was digested in nitric acid and H_2O_2 and the iron content in MY was analyzed by inductively coupled plasma optical emission spectroscopy (Perkin-Elmer, USA). The magnetic measurement was carried out with a vibrating sample magnetometer (Lakeshore 7307, USA). FTIR analysis was carried out using KBr pelletization method in the wavenumber range of 400–4000 cm^{-1} (Nicolet Nexus 670, USA). The particle size distribution was measured on laser diffraction particle size analyzer SALD-2200 (Shimadzu, Japan). The determination of point of zero charge pHzc was carried out according to the literature [15]. Briefly, eleven solutions of 0.1 mol/L NaCl were carefully to be adjusted to the range from 2.0 to 12.0 and composite was added to these solutions. The final pH of solution was plotted against initial pH value and the pHzc was determined as the point that pH value did not change after composite contacting.

2.4. Adsorption experiments

Stock As(V) solution (1000 mg/L) was prepared by dissolving $Na_2HAsO_4{\cdot}7H_2O$ in de-ionized water and desired solutions were prepared by dilution of the stock solution. The pH value of the solution was manually maintained for adsorption experiments in such a way that, the initial solutions was adjusted to preset value and then measured and adjusted at intervals of 2 h by nitric acid and sodium hydroxide (generally the pH did not show significant change after 6 h reaction). Adsorption experiments were carried out by batch method. For each experiment, 20 mg MY was weighed into 150-ml glass bottle and contacted with 100 ml of As(V) solutions. The bottles were sealed and placed in a shaker for until predetermined time was reached. The solutions were filtered and the concentrations of As(V) in the filtrate were determined by ICP-OES. The amount of As(V) adsorbed onto the adsorbent at time t, q_t (mg/g), was calculated as follows:

$$q_t = \frac{(C_{ini} - C_t)V}{W} \quad (1)$$

where C_{ini} and C_t (mg/L) are the initial and final concentration of As(V) at time t in the solutions, respectively, W (g) the amount of the adsorbent used and V (L) the volume of As(V) solution.

3. Results and discussion

3.1. Characterization of the composite MY

3.1.1. XRD studies

XRD patterns of MN and MY are presented in Fig. 1. The diffraction of MN does not show any peak thereby indicating the amorphous phase of the carbon prepared by the sulfuric acid activation. However, the formation of iron oxide phase with a spinel structure (magnetite, Fe_3O_4, or maghemite, γ-Fe_2O_3) is confirmed by the pattern of MY (peaks at 2θ = 18.30, 30.10, 35.30, 37.09, 42.90, 53.46, 56.76, 62.35) [16]. Taking into account the reducing atmosphere created by the sawdust pyrolysis, the γ-Fe_2O_3 can be reduced to Fe_3O_4 [17]. Therefore, it can be safely concluded that iron oxide in the MY was in the form of Fe_3O_4. The hypothesis was confirmed by the latter FTIR analysis. Besides, due to the overlap of the peaks, the diffraction peak centered at 2θ = 42.90 can be indexed with iron carbide Fe_2C formed at present pyrolysis process.

3.1.2. Morphology studies

SEM images shows that pores with different sizes and different shapes exist on external surfaces of both MN and MY as a result of sulfuric acid activation (Fig. 2). Unlike smooth surface of the MN, the surface of MY is much more coarse caused by the deposition of

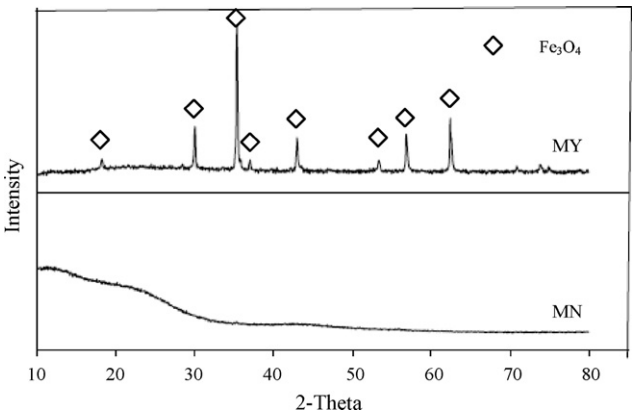

Fig. 1. X-ray diffraction patterns of MN and MY.

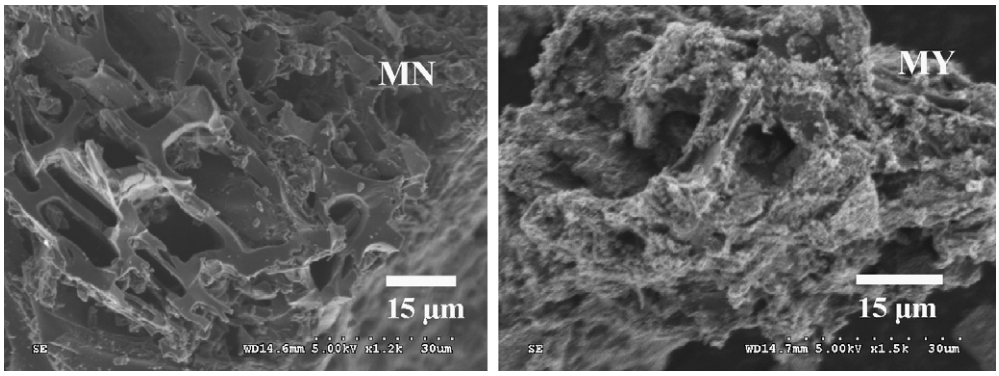

Fig. 2. SEM images of MN and MY.

Fig. 3. X-ray mapping of MY for Fe and O elements.

the Fe_3O_4 particles. Furthermore, two-dimensional X-ray mapping of selected zone of MY was carried out to investigate the distribution of Fe and O elements in the carbon matrix (Fig. 3). Most of Fe species identified as Fe_3O_4 was confirmed by the fact that the O signal is stronger than Fe signal and this result was in good agreement with the XRD observation. This analysis also revealed that Fe_3O_4 was almost uniformly deposited on the surface of the carbon.

3.1.3. FTIR analysis

The functional groups on the surface of MY and MN were investigated by FTIR spectra (Fig. 4). The FTIR spectra shows the shapes of both carbons are simple and similar and the main difference between them is that there is a broad adsorption band around 586 cm^{-1} in MY. This band was attributed to the stretching vibration and the torsional vibration of Fe–O bonds in the tetrahedral sites and in the octahedral sites of Fe_3O_4 [18]. The characteristic adsorption around 630 cm^{-1} was not observed in the FTIR spectrum, which suggested the absence of the γ-Fe_2O_3 in composite MY [18,19]. The band around 1500–1590 cm^{-1} in both MN and MY was assigned to ring vibration in a large aromatic skeleton or carbon–carbon double bonds generally found in activated carbons [20].

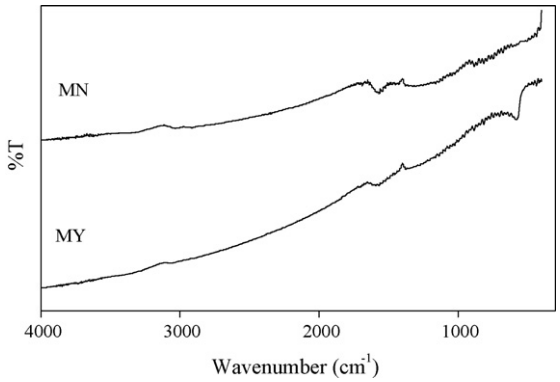

Fig. 4. FTIR spectra of MN and MY.

3.1.4. Surface area and pore properties

The porous property changed significantly due to the adding of $FeCl_3$ during the pyrolysis process and in comparison with MN, the BET surface area of MY decreased ca. 39% with surface area of 349 m^2/g and pore volume of 0.20 cm^3/g (Table 2). MN shows type-I adsorption isotherm indicating MN is predominant microporous and a relative small external surface area while isotherm of MY is an intermediate between type-II and type-IV, implying the presence of substantial mesopores in MY [21]. In addition the hysteresis loop of H3 showing non-limiting adsorption at high relative pressure suggested the slit-shaped porous nature of MY [21]. In spite of the Fe_3O_4 loading, the surface area of MY developed at present study exceeded or was comparable to some carbon materials from waste biomass reported in literature qualitatively [22–24].

Table 2
Physical properties of MN and MY and adsorption constants for As(V) onto the adsorbents.

Sample	MN	MY
Surface property		
Specific surface area (m^2/g)	572	349
Total pore volume (cm^3/g)	0.28	0.20
Fe (wt.%)	–	39
Saturation magnetization (emu/g)	–	47.67
Coercive force (Oz)	–	149.26
pHzc	–	7.05
Langmuir model		
q_{max} (mg/g)	43.7	204.2
$K_L \times 10^2$ (L/mg)	2.19	0.54
R^2	0.97	0.93
Freundlich model		
K_F ((mg/g)(L/mg)$^{1/n}$)	1.90	1.58
n	1.59	1.19
R^2	0.94	0.99

– Not available.

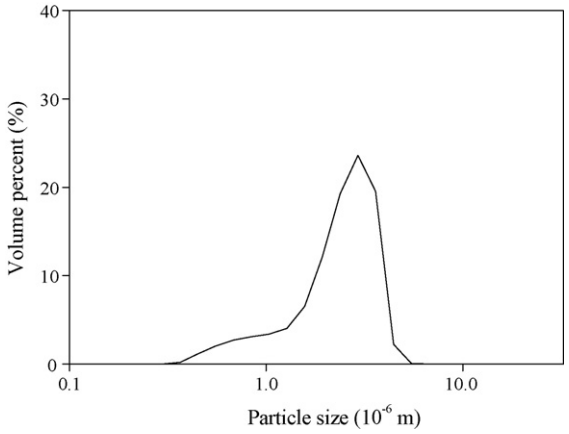

Fig. 5. Particle size distribution of the composite MY.

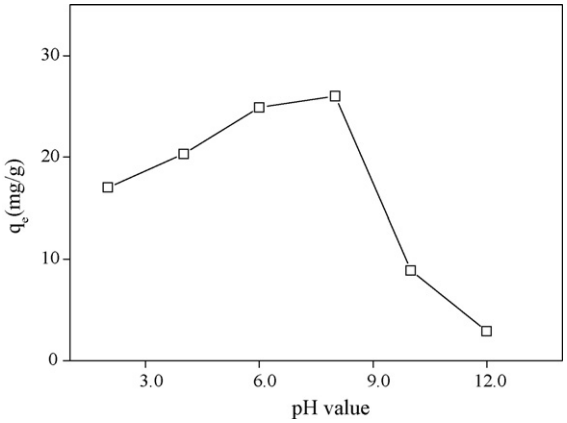

Fig. 6. Adsorption of As(V) onto MY as a function of solution pH (adsorbent dose 0.2 g/L; As(V) concentration 40 mg/L; temperature 303 K).

3.1.5. Magnetic properties

The particle size distribution of MY was analyzed and the result was shown in Fig. 5. According to the result, the composite particles distributed in the range from 0.30 to 5.48 μm with the mean particle size 1.98 μm. The small size MY dispersed in water can be removed easily by placing a conventional magnet near the beaker resulting in a clear solution. The detailed measurement results of magnetic property of MY by VSM shows that a characteristic hysteresis loop is present, indicating the ferromagnetic character of the sample. The saturation magnetization value is 47.67 emu/g, which is high enough to enable MY to be manipulated by the conventional magnets. The most significant results form the magnetic measurement for MY is the low coercive force H_C = 149.26 Oe and the ratio between the remanent and saturation magnetization ca. 0.20, indicating that this magnetic composite could be easily separated by an external magnetic field.

3.2. Adsorption of As(V) from aqueous solutions

3.2.1. Effect of pH on As(V) adsorption

The adsorption of As(V) onto MY as a function of pH was investigated to find the optimum pH value. The initial As(V) concentration was 40 mg/L and the contact time for As(V) adsorption was kept at 6 h. From Fig. 6, it can be seen that the As(V) adsorption is slightly increased with the increase of pH value and the maximum is achieved at the pH 8.0. As the pH is further increased, the adsorption decreases sharply and the adsorption capacity became very small at pH 12.0. The adsorption of As(V) onto MY is supposed to mainly through two routes: affinity adsorption and chemical reaction with Fe_3O_4 [25]. Affinity adsorption relates to the surface area of adsorbent while chemical reaction relates to the existing forms of the As(V) species. Considering the effect of pH, it can be safely concluded that the chemical reaction dominated the adsorption of As(V) onto MY. Taking into account of the fact that the surface of the composite MY was negatively charged at pH > pHzc 7.05 and increased negatively charge of As(V) at high pH value, the decrease trend of adsorption resulted from the enhanced electrostatic repulsion between the adsorbent MY and As(V) [26].

3.2.2. Kinetic study

The adsorption kinetic was investigated under different As(V) concentrations (10, 25, 40 mg/L) and temperatures (293, 303 and 313 K) at pH 8.0. It was found that the adsorption capacity increased along with the increase of temperature and initial As(V) concentration. The adsorption capacity increased with the increase of temperature, suggesting that As(V) adsorption onto MY was an endothermic process. Due to the sufficient energy provided by the promoted temperature, more As(V) reached and adsorbed onto MY interior structure, resulting in the higher adsorption capacity. As for the increase of adsorption with the increased initial As(V) concentration, it was explained by a higher probability of contact between the MY and As(V). Generally, the contact time for 95% removal equilibrium was less than 6 h under tested conditions. The data were analyzed according to the pseudo-first-order and pseudo-second-order equations. The kinetic parameters obtained from the analysis are shown in Table 3 and Fig. 7 shows the plots with initial As(V) concentration 40 mg/L at tested temperatures. As can be seen from the results, that adsorption kinetics for As(V) onto MY was best described by pseudo-second-order model.

3.2.3. Adsorption isotherms

The adsorption capacity of As(V) onto MY was evaluated through the determination of the adsorption isotherm (MN for comparison).

Table 3
Parameters of pseudo-first-order and pseudo-second-order kinetics models for As(V) adsorption onto MY.

Initial concentration (mg/L)	T (K)	Pseudo-first-order model $\log(q_e - q_t) = \log q_e - k_1 t/2.303$			Pseudo-second-order model $t/q_t = 1/(k_2 q_e^2) + t/q_e$		
		q_e	k_1	R^2	q_e	$k_2 \times 10^2$	R^2
10	293	4.7	0.40	0.90	4.8	11.2	0.99
	303	5.9	0.41	0.88	5.3	9.7	0.99
	313	6.8	0.44	0.94	6.0	7.8	0.99
25	293	10.3	0.33	0.96	12.6	6.2	0.98
	303	12.4	0.42	0.78	16.2	5.9	0.96
	313	11.9	0.35	0.83	21.3	4.6	0.99
40	293	13.8	0.19	0.96	28.9	2.9	0.99
	303	19.9	0.36	0.73	32.5	2.6	0.99
	313	20.0	0.34	0.63	35.6	2.2	0.99

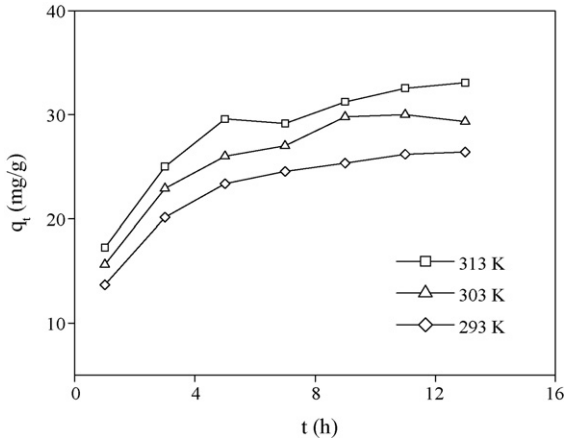

Fig. 7. Effects of contact time and temperature on As(V) removal capacity by MY (adsorbent dose 0.2 g/L; pH 8.0; As(V) concentration 40 mg/L).

In present study, Langmuir and Freundlich models are applied to describe the relationship between the amount of As(V) adsorbed and its concentration of equilibrium in solutions. The forms of the two isotherms are

$$\frac{C_e}{q_e} = \frac{1}{q_{max}K_L} + \frac{C_e}{q_{max}} \quad \text{Langmuir model} \tag{2}$$

$$\log q_e = \log K_F + \frac{1}{n}\log C_e \quad \text{Freundlich model} \tag{3}$$

where q_{max} (mg/g) is the maximum adsorption capacity of As(V) onto the composite, C_e (mg/L) the equilibrium concentration of the As(V), K_F (L/mg) and K_L ((mg/g)(L/mg)$^{1/n}$) the constants for Langmuir and Freundlich models, respectively.

Based on our preliminary experiments, a time of 24 h was used for adsorption isotherm at 303 K for achieving complete equilibrium and the results are displayed in Fig. 8 and Table 2. Within the examined concentration range (20–100 mg/L), As(V) adsorption capacities were 6.8–28.0 mg/g and 12.2–61.0 mg/g onto MN and MY, respectively. In comparison with MN, the adsorption data could be described well by the Freundlich model rather than Langmuir model for MY (R^2 was 0.93 and 0.99 for Langmuir and Freundlich fit, respectively). The well fitting of Freundlich was attributed to the fact that Freundlich expression is an empirical equation based on a heterogeneous surface while Langmuir model assumes that the adsorption of the metal ions occurs on a homogeneous surface by monolayer without any interaction between the adsorbate

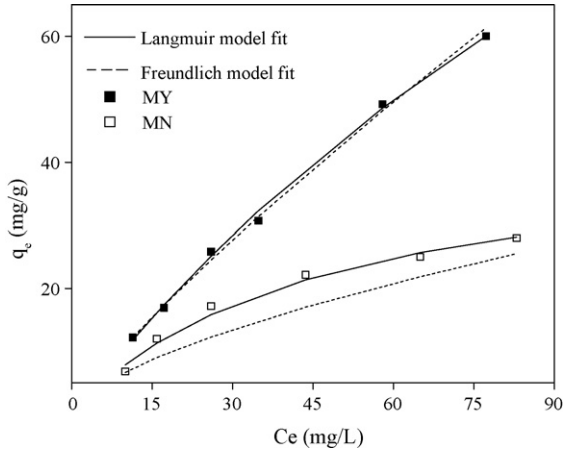

Fig. 8. Adsorption isotherms of As(V) onto MN and MY (temperature 303 K; adsorbent dose 0.2 g/L; pH 8.0).

Table 4
Comparison of the maximum monolayer adsorption of As(V) onto various adsorbents.

Adsorbent	Equilibrium pH	q_{max} (mg/g)	Reference
Fe_3O_4-loaded activated carbon	8.0	204	Present paper
Activated carbon MN	8.0	43.7	Present paper
Iron-containing granular activated carbon ($NaClO_2$)	4.7	6.57	[10]
Iron-modified activated carbon	8.0	43.6	[12]
Magnetite	8.0	172.5	[26]
Arc-carbon	6.4	30.5	[28]
Hydrous ferric oxide-granular activated carbon	7.5	10.5	[29]
Iron(III) loaded orange waste	10	68.6	[30]
Iron-containing mesoporous carbon (IMC)	7.9	5.2	[31]
Granular ferric hydroxide (GFH)	6.5	2.0	[32]

and adsorbent. The magnitude of the Freundlich exponent, n, is an indicator of the favorability of adsorption, with exponent values between $1 < n < 10$ showing a beneficial adsorption [27]. The Freundlich exponent, n, obtained in this study was 1.19, indicating a favorable As(V) adsorption onto MY. Various active sites and heterogeneous property on the surface of the composite MY led to different affinities to As(V), resulting in deviation of the Langmuir isotherm model. The values of q_{max} and K_L calculated from the Langmuir plots were 204.2 mg/g and 0.0054 L/mg, respectively.

Table 4 shows the comparison of the maximum monolayer adsorption capacities of various adsorbents for As(V) and the value of MY developed in present study is higher than MN and other adsorbents in previous studies. Taking into account of the high saturation magnetization, the MY developed in present study was an efficient magnetic adsorbent for As(V) removal from aqueous solutions.

4. Conclusions

A simple and versatile method for producing Fe_3O_4-loaded activated carbon (MY) which was effective for As(V) removal was successfully developed in this study. The composite, exhibiting large surface area of 349 m^2/g and 39 wt.% of iron content, was effective for As(V) adsorption. The maximum adsorption capacity for As(V) was 204.2 mg/g given by Langmuir model when 0.2 g/L MY was applied at 303 K. Furthermore, saturation magnetization of the composite was 47.67 emu/g, which allowed it to be removed easily by an external magnetic field.

This synthetic strategy offers two significant advantages: the starting materials are waste biomass, and the production of activated carbon and the loading of Fe_3O_4 are accomplished simultaneously through a simple step. Thus, it is believed that the proposed process is attractive for producing low-cost magnetic Fe_3O_4-contained composite and the developed composite is industrially applicable for As(V)-contaminated wastewater treatment.

Acknowledgements

This work was financially supported by the National S & T Major Project (2009ZX07212-002), National Basic Research Program (2007CB407303) and the National Key Technology R&D Program (2008BAC32B03) of China.

References

[1] W.R. Cullen, K.J. Reimer, Arsenic speciation in the environment, Chem. Rev. 89 (1989) 713–764.
[2] E.A. Deliyanni, D.N. Bakoyannakis, A.I. Zouboulis, K.A. Matis, Sorption of As (V) ions by akaganeite-type nanocrystals, Chemosphere 50 (2003) 155–163.
[3] M.L. Pierce, C.B. Moore, Adsorption of arsenite and arsenate on amorphous iron hydroxide, Water Res. 15 (1982) 1247–1253.
[4] P.R. Grossl, M. Eick, D.L. Sparks, S. Goldberg, C.C. Ainsworth, Arsenate and chromate retention mechanisms on goethite. 2. Kinetic evaluation using a pressure-jump relaxation technique, Environ. Sci. Technol. 31 (1997) 321–326.
[5] I.A. Katsoyiannis, A.I. Zouboulis, Removal of arsenic from contaminated water source by sorption onto iron oxide coated polymeric materials, Water Res. 36 (2002) 5141–5155.
[6] V.K. Gupta, V.K. Saini, N. Jain, Adsorption of As(III) from aqueous solutions by iron oxide-coated sand, J. Colloid Interf. Sci. 288 (2005) 55–60.
[7] P.B. Bhakat, A.K. Gupta, S. Ayoob, Investigation on arsenic (V) removal by modified calcined bauxite, Colloid Surf. A 281 (2006) 237–245.
[8] C.P. Huang, L.M. Vane, Enhancing As^{5+} removal by a Fe^{2+} treated activated carbon, J. Water Pollut. Control Fed. 61 (1999) 1596–1603.
[9] B.E. Reed, R. Vaughan, L.Q. Jiang, As (III), As (V), Hg and Pb removal by Fe-oxide impregnated activated carbon, J. Environ. Eng. 126 (2000) 869–873.
[10] Z. Gu, J. Fang, B. Deng, Preparation and evaluation of GAC-based iron-containing adsorbents for arsenic removal, Environ. Sci. Technol. 39 (2005) 3833–3843.
[11] J.R.L. Vaughan, B.E. Reed, Modeling As (V) removal by a iron oxide impregnated activated carbon using the surface complexation approach, Water Res. 39 (2005) 1005–1014.
[12] W. Chen, R. Parette, J. Zou, F.S. Cannon, B.A. Dempsey, Arsenic removal by iron-modified activated carbon, Water Res. 41 (2007) 1851–1858.
[13] G. Zhang, J. Qu, H. Liu, A.T. Cooper, R. Wu, $CuFe_2O_4$/activated carbon composite: a novel magnetic adsorbent for the removal of acid orange II and catalytic regeneration, Chemosphere 68 (2007) 1058–1066.
[14] N. Yang, S. Zhu, D. Zhang, S. Xu, Synthesis and properties of magnetic Fe_3O_4-activated carbon nanocomposite particles for dye removal, Mater. Lett. 62 (2008) 645–647.
[15] G. Muniz, V. Fierro, A. Celzard, G. Furdin, G. Gonzalez-Sánchez, M.L. Ballinas, Synthesis, characterization and performance in arsenic removal of iron-doped activated carbons prepared by impregnation with Fe(III) and Fe(II), J. Hazard. Mater. 165 (2009) 893–902.
[16] A.B. Fuertes, P. Tartaj, A facile route for the preparation of superparamagnetic porous carbons, Chem. Mater. 18 (2006) 1675–1679.
[17] A. Dufour, P. Girods, E. Masson, Y. Rogaume, A. Zoulalian, Synthesis gas production by biomass pyrolysis: effect of reactor temperature on product distribution, Int. J. Hydrogen Energy 34 (2009) 1726–1734.
[18] H. Namduri, S. Nasrazadani, Quantitative analysis of iron oxides using Fourier transform infrared spectrophotometry, Corros. Sci. 50 (2008) 2493–2497.
[19] R. Fu, W. Wang, R. Han, K. Chen, Preparation and characterization of [gamma]-Fe_2O_3/ZnO composite particles, Mater. Lett. 62 (2008) 4066–4068.
[20] Y. Guo, D.A. Rockstraw, Physicochemical properties of carbons prepared from pecan shell by phosphoric acid activation, Bioresour. Technol. 98 (2007) 1513–1521.
[21] K.S.W. Sing, D.H. Everett, R.A.W. Hanl, L. Moscou, R.A. Pirtotti, J. Rouquerol, et al., Deporting physisorption data for gas/solid system with special reference to the determination of surface area and porosity, Pure Appl. Chem. 57 (1985) 603–619.
[22] S. Karagoz, T. Tay, S. Ucar, M. Erdem, Activated carbons from waste biomass by sulfuric acid activation and their use on methylene blue adsorption, Bioresour. Technol. 99 (2008) 6214–6222.
[23] V. Sricharoenchaikul, C. Pechyen, D. Aht-ong, D. Atong, Preparation and characterization of activated carbon from the pyrolysis of physic nut (*Jatropha curcas* L.) waste, Energy Fuel 22 (2008) 31–37.
[24] N. Yalcin, V. Sevin, Studies of the surface area and porosity of activated carbons prepared from rice husks, Carbon 38 (2000) 1943–1945.
[25] F.S. Zhang, H. Itoh, Iron oxide-loaded slag for arsenic removal from aqueous system, Chemosphere 60 (2005) 319–325.
[26] S. Yean, L. Cong, C.T. Yavuz, J.T. Mayo, W.W. Yu, A.T. Kan, et al., Focus section: effect of magnetite particle size on adsorption and desorption of arsenite and arsenate, J. Mater. Res. 20 (2005) 3255–3256.
[27] R.E. Treybal, Mass Transfer Operations, McGrew-Hill, New York, 1998.
[28] J. Pattanayak, K. Mondal, S. Mathew, S.B. Lalvani, A parametric evaluation of the removal of As(V) and As(III) by carbon-based adsorbents, Carbon 38 (2000) 589–596.
[29] M. Jang, W. Chen, F.S. Cannon, Preloading hydrous ferric oxide into granular activated carbon for arsenic removal, Environ. Sci. Technol. 42 (2008) 3369–3374.
[30] K.N. Ghimire, K. Inoue, H. Yamaguchi, K. Makino, T. Miyajima, Adsorptive separation of arsenate and arsenite anions from aqueous medium by using orange waste, Water Res. 37 (2003) 4945–4953.
[31] Z. Gu, B. Deng, Use of iron-containing mesoporous carbon (IMC) for arsenic removal from drinking water, Environ. Eng. Sci. 24 (2007) 113–121.
[32] K. Banerjee, G.L. Amy, M. Prevost, S. Nour, M. Jekel, P.M. Gallagher, et al., Kinetic and thermodynamic aspects of adsorption of arsenic onto granular ferric hydroxide (GFH), Water Res. 42 (2008) 3371–3378.